Oral delivery of anti-MDM2 inhibitor SP141-loaded FcRn-targeted nanoparticles to treat breast cancer and metastasis

Jiang-Jiang Qin[a,b,*], **Wei Wang**[a,b,§,*], **Sushanta Sarkar**[a], and **Ruiwen Zhang**[a,b,§]

[a]Department of Pharmaceutical Sciences, School of Pharmacy, Texas Tech University Health Sciences Center, Amarillo, TX 79106, United State

[b]Cancer Biology Center, School of Pharmacy, Texas Tech University Health Sciences Center, Amarillo, TX 79106, United State

Abstract

We have recently discovered a specific Murine Double Minute 2 (MDM2) oncogene inhibitor, called SP141, which exerts potent anticancer activity in various breast cancer models. However, its low oral bioavailability is the major hurtle for moving this drug to clinical trial. The present study was designed to discover and validate a novel nano-oral delivery system for this promising anticancer agent. Herein, we report the preparation, characterization, and evaluation of the efficacy and safety of the SP141-loaded IgG Fc-conjugated maleimidyl-poly(ethylene glycol)-co-poly(ε-caprolactone) (Mal-PEG-PCL) nanoparticles (SP141FcNP) as an orally cancer therapeutic agent. Our results indicated that SP141FcNP showed a biphasic release pattern and increased transepithelial transport *in vitro* and *in vivo* with the involvement of FcRn-mediated transcytosis. SP141FcNP also exhibited increased intestinal epithelial permeability, cellular uptake, and oral bioavailability, with extended blood circulation time, increased tumor accumulation, enhanced MDM2 inhibition, and stronger responses in anti-tumor growth and metastasis effects *in vitro* and *in vivo*, without apparent host toxicity. Collectively, this newly developed nanoparticle oral delivery system provides a basis for evaluation of SP141 as a potential clinical candidate for cancer therapy.

Keywords

§**Correspondence and requests for reprints:** Dr. Wei Wang, MD, PhD, Department of Pharmaceutical Sciences, School of Pharmacy, Texas Tech University Health Sciences Center, 1406 S. Coulter Dr. Suite 1104, Amarillo, TX 79106, USA; wwei.wang@ttuhsc.edu; Tel: 806-414-9246; or Dr. Ruiwen Zhang, MD, PhD, DABT, Department of Pharmaceutical Sciences, School of Pharmacy, Texas Tech University Health Sciences Center, 1406 S. Coulter Dr. Suite 1116, Amarillo, TX 79106, USA; ruiwen.zhang@ttuhsc.edu; Tel: 806-414-9248.
*These authors contributed to this work equally.

1. Introduction

Recent advances in our understanding of genetic alterations in human cancer have improved the diagnosis, prevention, and treatment of this disease [1–3]. The amplification and overexpression of Murine Double Minute 2 (MDM2) oncogene and the mutation and deletion of p53 tumor suppressor often occur in human cancers, including breast cancer [4–6]. Inhibiting MDM2 and/or reactivating p53 hold great promise in developing targeted therapies for patients with advanced cancer [6–8]. A number of MDM2 inhibitors have recently been developed to treat human cancers [9–13]. However, challenges remain in the pursuit of specific, safe, and effective MDM2 inhibitors for cancer therapy, such as low targeting specificity, poor bioavailability, host toxicity, and limited efficacy. We have recently discovered a novel small molecule MDM2 inhibitor SP141 with a unique molecular mechanism that is distinct from other MDM2 inhibitors under development [12, 14]. SP141 directly interacts with MDM2 and induces MDM2 autoubiquitination and proteasomal degradation, leading to cancer cell death, regardless of p53 status [12, 14]. However, the therapeutic applications of SP141 are restricted by moderate efficacy through oral administration, due to the poor aqueous solubility and instability under harsh conditions. Therefore, new strategies for directed and efficient delivery of SP141 are needed.

Owing to the chronic and aggressive nature of cancers, long-term treatment with medication is often required and the oral administration route is preferred because of its convenience and non-invasiveness [15]. Recently, the advent of nanotechnology and nanomedicine has demonstrated great promise for advancing the treatment of various cancers by improving the specificity and efficacy of therapeutics and reducing adverse effects [16–18]. The bench-to-bedside translation of several nanomedicines, such as CPX-351 (NCT00822094) and BIND-014 (NCT01300533) further emphasizes that the therapeutic potential of nanomedicine is superior to that of conventional cancer therapies [19–21]. However, the utilization of nanomedicine approaches for enhancing oral delivery of anticancer drugs is still lacking, and more specific, safe, and effective oral nanomedicine is needed for cancer therapy. More recently, a multitude of nanoparticle formulations have been developed to encapsulate and protect drugs from premature degradation in gastric environment, resist the harsh conditions, and release the drugs in the intestine in a controlled manner, leading to an increased absorption of free drugs [22–24]. Nevertheless, the physicochemical properties of nanoparticles are unfavorable for the transport of the intact nanoparticles across cellular barriers, such as intestinal epithelial cells; the intestinal absorption of the drugs is still restricted and highly inefficient [15, 25, 26]. Therefore, new strategies are urgently needed for overcoming the intestinal epithelial barrier and improving the absorption efficiency of nanomedicines.

The neonatal Fc receptor (FcRn) was originally discovered as a specific receptor for Immunoglobulin G (IgG), protecting IgG from degradation and extending its half-life in the serum via FcRn-mediated recycling and transcytosis [27, 28]. Mechanistically, FcRn binds to the Fc portion of IgG in a pH-dependent manner. At the moderate acid condition (*e.g.* intestinal juices, pH < 6.5), the acidic residues on the α2-domain of FcRn specifically interacts with the titratable histidine residues in the Fc C_H2-C_H3 domains via electrostatics, whereas the FcRn-Fc interaction will be dissociated at physiological pH condition (pH 7.4)

[27, 28]. FcRn is highly expressed in intestinal epithelium, vascular endothelium, and various sites in human body, and is involved in diverse biological functions throughout human life [29–32]. Recent studies have demonstrated that the conjugation of IgG Fc portion to nanoparticles can enhance the intestinal absorption of the intact nanoparticles and extend their serum persistence, leading to improved oral bioavailability and increased tissue accumulation of drugs, *e.g.*, insulin [33, 34]. However, the specificity, safety, and efficacy of FcRn-targeted anticancer nanomedicine remain unclear.

In the present study, we designed and developed the SP141-encapsulated FcRn-targeted nanoparticles (SP141FcNP) with well-controlled formulation properties for oral delivery of this MDM2 inhibitor. To facilitate the transition of SP141FcNP from preclinical to clinical studies, we selected the biodegradable and biocompatible maleimidyl-poly(ethylene glycol)-co-poly(ε-caprolactone) (Mal-PEG-PCL) copolymers and anti-human IgG Fc portion for preparing the antibody-nanoparticle conjugates. The PEGylated polymers were employed to prolong circulation, decrease non-specific absorption, and reduce nanoparticle aggregation *in vivo*. SP141FcNP was investigated using various *in vitro* and *in vivo* models that are useful in modeling the harsh environment of the gastrointestinal tract. Considering that SP141 has shown excellent efficacy in *in vitro* and *in vivo* breast cancer models [12], the same models, including breast cancer orthotopic model, were utilized to assess the safety, tumor targeting efficiency, and anticancer activity of SP141FcNP in the present study. Our results have shown the feasibility of Fc-conjugated nanoparticle as an oral delivery system of SP141 for cancer therapy. This study is highly significant and paves the way for further development of SP141 for treating human cancer.

2. Materials and methods

2.1. Chemicals, antibodies, and reagents

The small molecule MDM2 inhibitor SP141 was synthesized and characterized as described in our previous studies [12, 14]. The Mal-PEG-PCL copolymers (6 KDa) were purchased from Advanced Polymer Materials (Montreal, Canada). Human IgG Fc fragments were sourced from Jackson ImmunoResearch Laboratories (West Grove, PA, USA). 2-Iminothiolane hydrochloride was obtained from Sigma (St Louis, MO, USA). DilC$_{18}$(5) oil (1,1'-dioctadecyl-3,3,3',3'-tetramethylindodicarbocyanine perchlorate) was purchased from Thermo Scientific (Rockford, IL, USA). Fetal bovine serum was obtained from Atlanta Biologicals (Lawrenceville, GA, USA). The penicillin/streptomycin was bought from Corning (Manassas, VA, USA). The antibodies against human p53 (DO-1; 1:2000) and FcRn (H-4; 1:1000) were purchased from Santa Cruz Biotechnology (Santa Cruz, CA, USA). The antibodies against human MDM2 (Ab-2; 1:500) and p21 (Ab-1; 1:1000) were bought from EMD Chemicals (Gibbstown, NJ, USA). The goat antimouse IgG (H+L) and goat anti-rabbit IgG (H+L) antibodies were obtained from Bio-Rad (Hercules, CA, USA).

2.2. Cell lines and culture conditions

Human intestinal epithelial Caco2 cells, human non-malignant breast epithelial MCF10A cells, and human breast cancer cell lines (MCF7 and MDA-MB-231) were obtained from American Type Culture Collection (Rockville, MD, USA). Human mammary luminal

epithelial (HMLE) cells were obtained from ZenBio (Research Triangle Park, NC, USA). Caco2 cells were grown in Eagle's minimum essential medium (EMEM). MCF7 and MDA-MB-231 cells were cultured in Dulbecco's modified Eagle's medium (DMEM). Both EMEM and DMEM were supplemented with 10% fetal bovine serum and 1% penicillin/streptomycin. MCF10A cells were grown in DMEM/Ham's F12 media containing 5% horse serum, 20 ng/mL of EGF, 0.5 mg/mL of hydrocortisone, 100 ng/mL of cholera toxin, 10 μg/mL of insulin, and 1% penicillin/streptomycin. HMLE cells were grown in mammary luminal epithelial cell growth medium (ZenBio, NC, USA).

2.3. Preparation and characterization of nanoparticles

To prepare SP141-loaded nanoparticles, Mal-PEG-PCL copolymers (15.0 mg) and SP141 (3.0 mg) were dissolved in 1 mL dichloromethane, and then added dropwise into 5 mL of deionized water. The mixture was sonicated on ice using a probe sonicator to form the w/o emulsion. After that, the organic solvent in the mixture was evaporated by continuous stirring at room temperature overnight. The nanoparticles were then purified by filtration using Millipore Amicon Ultra 100,000 NMWL (Millipore, Billerica, MA, USA).

The Fc-conjugated nanoparticles were prepared as reported previously [33, 34]. Briefly, IgG Fc fragments were first thiolated by reacting with 2-iminothiolan (Traut's reagent). The thiolated Fc fragments were added into Mal-PEG-PCL nanoparticle suspensions containing 5 mM EDTA and mixed for covalent conjugation at 4°C for 1 h. The FcNPs were washed and purified using Millipore Amicon Ultra 100,000 NMWL. The conjugation efficiency of IgG Fc to nanoparticle surface and the average number of Fc fragments conjugated to each nanoparticle were determined as reported previously [35]. The nanoparticles loaded with fluorescent dye DiD were prepared in the same way.

The size distribution and zeta potential of the nanoparticles were determined using dynamic light scattering (Zetasizer 3000HS, Malvern Instruments Ltd, UK). The morphology of the nanoparticles was examined using transmission electron microscopy (TEM) (Hitachi H-9500, Hitachi High Technologies America, Dallas, TX, USA). The drug loading, encapsulation efficiency, and *in vitro* release kinetics of the nanoparticles were determined using the previously reported methods [24].

2.4. Caco2 cell monolayer permeability assays

The Caco2 cell monolayer permeability assay was performed as described previously [24]. In brief, Caco2 cells were seeded on polycarbonate 6-well Transwell® inserts (Corning Costar, NY, USA). The transepithelial electrical resistance (TEER) of the monolayer was monitored using an epithelial voltohmmeter (EVOM, WPI, USA). Free SP141 (5 μg/mL), SP141NP (5 μg/mL), or SP141FcNP (5 μg/mL) were added to the apical side of the membrane, and the transport of the compound from the apical compartment to the basolateral compartment was monitored over a 120 min time period using an HPLC method [36]. For the competition assay, the cells were pretreated with IgG Fc fragments for 30 min, followed by the addition of SP141FcNP. The amount of Fc fragments transported was determined using the human IgG Fc ELISA kit (eBioscience, San Diego, CA, USA). The apparent permeability coefficient (P_{app}) was calculated using the following equation: P_{app} =

($\Delta Q/\Delta t)/(A \times C_0)$, where '$\Delta Q/\Delta t$' is the permeability rate of the compound across the cells, 'A' is the diffusion area of the cell monolayer and 'C_0' is the initial concentration of the compound in the apical compartment.

2.5. In vitro cellular uptake assays

The uptake of nanoparticles into Caco2, MCF7, and MDA-MB-231 cells was determined by HPLC analyses and fluorescence detection as reported previously [24]. For the quantitative analyses of cellular uptake of SP141-loaded nanoparticles, the cells were incubated with 5 μg/mL of free SP141, SP141NP, or SP141FcNP for 30, 60, and 120 min. The cells were then frozen at −80°C overnight and cell lysates were collected and extracted for the quantification of SP141 by an HPLC analysis [36]. For fluorescence detection, cells were incubated with free DiD, DiD-NP, and DiD-FcNP for 2 h and then fixed using 4% formalin in PBS. In the competition assay, the cells were pretreated with IgG Fc fragments for 30 min, followed by the addition of SP141FcNP. The cells were stained with membrane lipophilic dye using CellVue® Jade Cell Labeling kit following the manufacturer's instructions (eBioscience, San Diego, CA, USA). After labeling, the cells were then counterstained with 4', 6-diamidino-2-phenylindole (DAPI) and analyzed under an Olympus fluorescence microscope (Olympus America, Central Valley, PA, USA).

2.6. Assays for in vitro anticancer activity

Assays for cell viability, cell cycle distribution, and cell apoptosis were performed as described previously [37, 38]. In brief, the cells were seeded in 96-well plates ($3–4 \times 10^3$ cells/well) and treated with various concentrations of SP141, SP141NP, and SP141FcNP for 72 h to examine their cytotoxicity using the MTT assay. For cell cycle assay, the cells ($2–3 \times 10^5$ cells/well) were exposed to the formulations (0, 20, 50, and 100 ng/mL) for 24 h and then harvested and fixed at 4°C overnight. The DNA content was determined using a FACSCalibur flow cytometer (BD Biosciences, San Jose, CA, USA). For cell apoptosis detection, the cells ($2–3 \times 10^5$ cells/well) were treated with the formulations (0, 20, 50, and 100 ng/mL) for 48 h, followed by staining and analysis using flow cytometry.

2.7. Western blotting assay

In the *in vitro* studies, $3–4 \times 10^5$ cells were seeded into 6-cm dishes and exposed to various concentrations of SP141, SP141NP, and SP141FcNP (0, 20, 50, and 100 ng/mL) for 24 h. The cells were then lysed in NP-40 lysis buffer containing a protease inhibitor mixture (Sigma, St. Louis, MO, USA). In the *in vivo* studies, the tumor tissue samples were homogenized in NP-40 lysis buffer and the supernatants were collected. The proteins from cell and tissue lysates were quantified, and the protein samples were then subjected to Western blotting analysis for the expression levels of MDM2, p53, and p21 using the methods described previously [39, 40].

2.8. MDA-MB-231 orthotopic tumor model and in vivo efficacy studies of SP141FcNP

The animal protocols were approved by the Institutional Animal Use and Care Committee of Texas Tech University. Female athymic nude mice (nu/nu, 4–6 weeks) were obtained from Charles River Laboratories International (Wilmington, MA, USA). MDA-MB-231 cells (1 ×

10^6 in 20 μL) were implanted into the second thoracic mammary fat pad after anesthesia. After two weeks, tumor-bearing mice were divided into control and treatment groups (10 mice/group). Free SP141 was dissolved in PEG400:ethanol:saline (57.1:14.3:28.6, *v:v:v*). The control group received the vehicle only. Both free SP141 and SP141NP were administered by oral gavage at a dose of 160 mg/kg/day, 5 days/week for 24 days. SP141FcNP was administered at a dose of 80 or 160 mg/kg/day for the same treatment period as SP141 and SP141FcNP. At the end of the experiments, all mice were examined for tumor metastasis to various organs. The numbers of mice with metastasis to the lungs were counted. Orthotopic tumors were removed, and parts of the tumors were snap frozen and used for Western blotting analysis, while other parts were fixed in formalin and used for immunohistochemistry and TUNEL staining. Various tissues (lungs, brain, heart, liver, spleen, and kidneys) were removed and fixed for hematoxylin and eosin (H&E) staining.

2.9. In vivo intestinal uptake studies of nanoparticles

To observe the *in vivo* transport of nanoparticles across the intestinal epithelium, both CD-1 mice and nude mice were fasted overnight and administrated with free DiD, DiD-NP, or DiD-FcNP at the dose level of 0.5 mg/kg by oral gavage. After 2 h, the mice were euthanized and the duodenum tissue sections were collected and frozen into Tissue-Tek OCT using liquid nitrogen. Cross sections of the tissues were obtained using a Shandon SME Cryotome Cryostat (Shandon Scientific Ltd, Runcorn, Cheshire, UK) with a thickness of 20 μm. After air-dried overnight, the tissue sections were fixed and stained with DAPI. Fluorescent images were obtained using an Olympus microscope (Olympus America, Central Valley, PA, USA).

2.10. Pharmacokinetics and tumor uptake of SP141FcNP

Pharmacokinetic studies of SP141FcNP were carried out in CD-1 mice and nude mice bearing MDA-MB-231 orthotopic tumors as described in our previous studies [24, 41]. Briefly, CD-1 and tumor-bearing nude mice were divided randomly into three groups and given SP141 in PEG400:ethanol:saline (57.1:14.3:28.6, *v:v:v*), SP141NP, and SP141FcNP at a dose of 160 mg/kg by oral administration. The plasma and tumor tissues were collected at 0, 0.5, 1, 2, 4, 6, 12, 24, 48, 72, and 96 h after treatment. The plasma and tumor samples were stored at −80°C until HPLC analyses.

2.11. In vivo imaging in CD-1 mice and tumor-bearing nude mice

To observe the real-time biodistribution and tumor accumulation of nanoparticles *in vivo*, CD-1 mice and nude mice bearing MDA-MB-231 tumors (~500 mg) were administrated free DiD in PEG400:ethanol:saline (57.1:14.3:28.6, *v:v:v*), DiD-NP, or DiD-FcNP at a dose of 0.5 mg/kg by oral gavage. The mice were anesthetized and scanned at 30 min, 1 h, 2 h, 4 h, 6 h, 8 h, 12 h, 24 h and 48 h using an IVIS Lumina XR *in vivo* imaging system (Caliper, Mountain View, CA, USA) with an excitation bandpass filter at 640 nm and an emission at 720 nm. Representative mice were selected from each treatment group and necropsy was conducted at 6 h. The major organs (brain, lungs, livers, spleen, kidneys, heart, stomach, and intestine) and tumor tissues were excised and the near-infrared fluorescence signal intensities in different tissues were measured.

2.12. Immunohistochemistry, TUNEL staining, and H&E staining

At the end of the *in vivo* experiments, tumors and different tissues were removed from the mice, fixed in 10% formalin and embedded in paraffin. Tumor and tissue sections with a thickness of 5 μm were deparaffinized in xylenes, rehydrated, and washed with PBS. For the immunohistochemistry studies [39, 40], the tumor slides were incubated with a biotinylated antihuman MDM2 antibody (diluted 1:50 in 5% BSA in PBS) for 1 h at room temperature. For TUNEL staining [39, 40], tissue sections were incubated with proteinase K (20 μg/mL in 10 mM Tris-HCl, pH 7.4) for 15 min at 37°C. DNA breaks were then labeled with terminal deoxytransferase (TdT) in a humidified chamber at 37°C for 5 min, followed by incubation with 50 μL of biotinylated bromodeoxyuridine antibody at 37°C for 1 h, and washing with PBS. Staining for both immunohistochemistry and TUNEL assay was developed with streptavidin-conjugated HRP and 3,3′-diaminobenzidene (an HRP substrate). For H&E staining [13], tissue sections were stained in Mayer's hematoxylin for 10 min, followed by eosin staining for less than 1 min. All the slides were analyzed and viewed under phase-contrast Olympus microscope (Olympus America, Central Valley, PA).

2.13. Statistical analysis

All quantitative data are reported as the means ± SEM from at least three independent experiments. The Prism software program version 6 (Graph Pad software, San Diego, CA, USA) was used for the data analysis. The Student's two-tailed *t*-tests were used for comparisons between two groups. $P < 0.05$ was considered to be statistically significant.

3. Results

3.1. SP141FcNP is a highly controllable formulation

SP141 was encapsulated into Mal-PEG-PCL nanoparticles using emulsion-solvent evaporation method (Fig. 1A), forming SP141-loaded nanoparticles (SP141NP) with a mean hydrodynamic diameter of 79.9 nm, a low polydispersity (PDI < 0.3), and a zeta potential of −7.2 mV (Table 1). The SP141NP exhibited spherical shape of moderate uniform particle size. The particle size and size distribution measured by the dynamic light scattering (DLS) (Fig. 1B) were in good agreement with that measured from TEM (Fig. 1C). The SP141 loading and encapsulation efficiency were 16.5% and 98.9%, respectively (Table 1). The *in vitro* cumulative release profile of SP141 from SP141NP was assessed at physiological pH condition (pH 7.4), in simulated intestinal fluid (pH 6.5), and in simulated gastric fluid (pH 1.2). SP141NP showed a biphasic release pattern at these pH conditions (Fig. 1D). After the initial burst release for 24 h, the release rate of SP141 from SP141NP significantly slowed down and exhibited a sustained release profile in the next six days.

The free maleimide groups of SP141NP specifically reacted with the thiol groups of the polyclonal IgG Fc fragments, forming the SP141-loaded Fc-conjugated PEG-PCL nanoparticles (SP141FcNP) (Fig. 1A). The Fc conjugation efficiency was determined to be 57.9% and the average number of Fc portion per SP141NP was 52 (Table 1). Since the Fc fragments (~3 nm) were covalently bound on the SP141NP surface, the hydrodynamic diameter of SP141FcNP was increased to 85.5 nm (PDI < 0.3), as measured by DLS (Fig. 1E) and TEM (Fig. 1F). However, only minor changes in zeta potential, SP141 loading, and

encapsulation efficiency were observed (Table 1). In addition, SP141FcNP presented a similar biphasic release profile as SP141NP at different pH conditions (Fig. 1G), indicating that IgG Fc conjugation to nanoparticles did not change the release behavior of SP141NP. Taken together, SP141FcNP was developed with controlled formulation properties, including narrow size distribution, high SP141 loading and biphasic release pattern.

3.2. SP141FcNP exhibits increased transepithelial transport and cellular uptake in vitro and in vivo

FcRn is highly expressed in the epithelium of the intestinal villi of the duodenum of mice [34]. SP141 exerts its anticancer activity by inhibiting MDM2 *in vitro* and *in vivo* [12, 14]. To determine the roles of FcRn and MDM2 in intestinal epithelial transport and cellular uptake of SP141FcNP, we first examined the expression levels of FcRn and MDM2 in human intestinal epithelial Caco2 cells, normal human breast epithelial cell lines (HMLE and MCF10A), and human breast cancer cell lines (MCF7 and MDA-MB-231). As shown in Fig. 2A, FcRn was highly expressed in all cell lines, whereas MDM2 was only overexpressed in breast cancer cell lines.

The *in vitro* transepithelial transport of SP141FcNP was evaluated using the Caco2 cell monolayer permeability assay. As shown in Fig. 2B (left panel), the results from human IgG Fc ELISA assays showed that SP141FcNP crossed the Caco2 monolayer in a time-dependent manner and preincubation of free Fc fragments reduced the transport of SP141FcNP, suggesting an involvement of FcRn-mediated transcytosis in the transport of the nanoparticles. The results from HPLC analyses (Fig. 2B, right panel) indicated that SP141FcNP had better transepithelial permeability ($P_{app} = 29.1 \times 10^{-5}$ cm/s) than both free SP141 ($P_{app} = 7.0 \times 10^{-5}$ cm/s) and non-targeted SP141NP ($P_{app} = 15.5 \times 10^{-5}$ cm/s). Furthermore, the transported SP141FcNP was evidently reduced after adding the free Fc fragments ($P_{app} = 18.2 \times 10^{-5}$ cm/s), confirming an important role of FcRn in the transepithelial transport of SP141FcNP.

The cellular uptake of SP141FcNP by Caco2 cells and breast cancer MCF7 and MDA-MB-231 cells was further investigated. Similar to the observations in permeability assays, SP141FcNP showed the best cellular uptake in all three cell lines in a time-dependent manner (Fig. 2C). The addition of free Fc fragments significantly reduced the uptake of SP141FcNP in all cell lines (Fig. 2C). These results were further confirmed using fluorescent dye DilC$_{18}$(5) oil (DiD)-loaded nanoparticles (DiD-NP). As shown in Fig. 2D, free DiD oil was unable to diffuse into the cells whereas DiD-NP showed accumulation in all cell lines. The DiD-loaded Fc-conjugated nanoparticles (DiD-FcNP) was actively accumulated into all different types of cells via binding to the cell surface and being uptaken by the cells, resulting in the most intense fluorescence in all cell lines, which was also reduced by adding the free Fc fragments. All these results suggested that FcRn played a crucial role in the cellular uptake of SP141FcNP, which was not affected by the different expression levels of MDM2 in these cell lines.

Furthermore, to determine the *in vivo* permeability and cellular uptake of SP141FcNP in intestine, both CD-1 mice and nude mice were orally administered free DiD oil, non-targeted DiD-NP, and DiD-FcNP, and the sections of the duodenum were fixed and

examined using confocal fluorescence microscopy. As shown in Fig. 2E, the fluorescence was not observed in the villi from the free DiD-treated group and it was only rarely observed in the DiD-NP group for both mouse models. However, the distribution of DiD fluorescence in the villi on the basolateral side of the epithelial cells was clearly observed in the mice treated with DiD-FcNP. Taken together, all these findings suggested that SP141FcNP could cross the intestinal epithelium and be uptaken by normal and breast cancer cells *in vitro* and *in vivo*.

3.3. SP141FcNP demonstrates increased anti-breast cancer activity and enhanced MDM2 inhibition in vitro, independent of p53

Two breast cancer cell lines MCF7 (FcRn high, MDM2 high, and p53 wild-type) and MDA-MB-231 (FcRn high, MDM2 high, and p53 mutant) were selected to determine the *in vitro* anticancer activity of SP141FcNP. As shown in Fig. 3A, SP141FcNP induced a significant increase in the cancer cell death in comparison to free SP141 and non-targeted SP141NP, resulting in a ~90% decrease in the IC_{50} values in both cell lines. The effects of SP141FcNP on cell cycle progression were further investigated in both cell lines. As shown in Fig. 3B, free SP141 only induced G2/M phase arrest at the highest concentration (100 ng/mL), whereas SP141NP and SP141FcNP started to induce cell cycle arrest at 50 and 20 ng/mL, respectively. Similar results were obtained in the cell apoptosis after 48 h posttreatment with SP141, SP141NP, and SP141FcNP (Fig. 3C). In comparison to SP141 or SP141NP, treating both cell lines with SP141FcNP at the same concentration significantly increased the apoptotic cells, regardless of p53 status.

Consistent with the results of cell cycle distribution and apoptosis, SP141FcNP inhibited the MDM2 expression and activated wild-type p53 and p21 expression at 20 ng/mL, while both free SP141 and non-targeted SP141NP did not show significant effects at the same concentration (Fig. 3D). Because FcRn is highly expressed in both MCF7 and MDA-MB-231 cell lines, the enhanced activity of SP141FcNP could be attributed to FcRn-mediated endocytosis. Taken together, these results demonstrated that SP141FcNP was uptaken by breast cancer cells via, at least in part, FcRn-mediated endocytosis and exerted its anticancer activity in a p53-independent manner.

3.4. SP141FcNP displays substantially altered pharmacokinetics in vivo

To determine the optimal therapeutic dose of SP141FcNP in *in vivo* studies, the initial short-term toxicity studies were performed using CD-1 mice. No mortality was observed in all the tested mice at two dose levels (160 and 320 mg/kg, p.o.) during the experimental period. No abnormal clinical observations were noticed as well, including decreases in food consumption, loss of average body weights, and organ abnormalities (Data not shown).

SP141FcNP was further evaluated for its *in vivo* pharmacokinetics in female CD-1 mice. As shown in Fig. 4A, oral administration of free SP141 (160 mg/kg) only caused very low drug concentrations in the plasma with a peak value (C_{max}) of 4.3 μg/mL one hour after dosing. SP141NP significantly increased the plasma concentration of this compound (C_{max} = 8.1 μg/mL) without changing the time point of the peak value (T_{max}). However, oral administration of SP141FcNP resulted in a dramatically altered pharmacokinetic profile,

with the highest drug concentration of 15.5 μg/mL at 4 h. Because of FcRn-mediated serum persistence of SP141FcNP, its plasma half-life ($T_{1/2}$) was extended to more than 24 h and SP141 was still detectable at 72 h. The AUC_{0-t} (the area under the concentration-time curve from the time zero to last measurable concentration) value for SP141FcNP was 32-fold higher than that of free SP141, indicating a greatly improved oral bioavailability. The selected pharmacokinetic parameters for SP141, SP141NP, and S141FcNP in CD-1 mice were summarized in Fig. 4B.

We further evaluated the *in vivo* pharmacokinetics and tumor uptake of SP141FcNP in nude mice bearing MDA-MB-231 orthotopic tumors. As shown in Fig. 4C, similar plasma concentration-time profiles to that from CD-1 mice were obtained, suggesting that there were no significant strain-related variations. In comparison to SP141- and SP141NP-treated mice, a larger amount of SP141 was measured in the tumor tissues from SP141FcNP-treated mice (Fig. 4D), indicating that more SP141FcNP entered into the systemic circulation and reached MDA-MB-231 tumor tissues. These results were supported by the pharmacokinetic parameters for all three formulations in the tumor-bearing nude mice (Fig. 4E). We also analyzed the biodistribution of SP141, SP141NP, and SP141FcNP in various tissues, including liver, lungs, kidneys, spleen, heart, and brain from both CD-1 mice (Supplementary Fig. 1) and tumor-bearing nude mice (Fig. 5). The significantly increased SP141 accumulation by Fc-conjugated nanoparticles was observed in all of the tissues. The pharmacokinetic parameters for all three formulations in the tissues from both CD-1 mice and nude mice were shown in Supplementary Table 1.

Taken together, these data suggested that the encapsulation of SP141 by Fc-conjugated nanoparticles substantially improved the oral bioavailability of this compound, extended its serum half-life and increased its tumor and tissue accumulation *in vivo*.

3.5. FcNP formulation enhances tumor uptake and tissue accumulation in vivo

We further investigated the real-time biodistribution and tumor accumulation ability of DiD-FcNP in both CD-1 mice and nude mice bearing MDA-MB-231 orthotopic tumors. Compared with free DiD and non-targeted DiD-NP, the fluorescence signals of DiD-FcNP in whole bodies of both strains of mice were the highest at all time points post-administration (Supplementary Fig. 2A and Fig. 6A, respectively). After two hours post-administration, obviously stronger fluorescent signals were observed in the tumors of mice from DiD-FcNP group and maintained up to 48 h (Fig. 6A). To compare the real-time tissue accumulation of DiD in the bodies of the mice, representative mice were selected from each group and necropsy was conducted at 6 h. Tumor tissues and major organs (brain, lungs, livers, spleen, kidneys, heart, stomach, and intestine) were collected and examined by the *ex vivo* imaging. The strongest fluorescence intensity was found in DiD-FcNP treatment group (Fig. 6B). Similar results were obtained from CD-1 mice (Supplementary Fig. 2B).

3.6. SP141FcNP displays enhanced efficacy in nude mice bearing orthotopic breast tumors in vivo

The *in vivo* efficacy of SP141FcNP was finally evaluated using the MDA-MB-231 orthotopic model of human breast cancer. As shown in Fig. 7A, free SP141 was orally

administered at dose of 160 mg/kg/day for 24 days and only had moderate inhibitory effects on tumor growth, resulting in 51% inhibition of the MDA-MB-231 tumor growth. SP141NP at the same dose level showed better efficacy in inhibiting the tumor growth (68% inhibition at Day 24). However, treating the tumor-bearing mice with 80 and 160 mg/kg of SP141FcNP led to approximately 79% and 90% inhibition in tumor growth, respectively. More importantly, the complete tumor regression was observed in the mice treated with 160 mg/kg of SP141FcNP. In addition, no significant loss of body weight in any treatment groups was observed during the treatment period, suggesting that these treatments did not lead to host toxicity (Fig. 7B).

We further evaluated the expression level of MDM2 *in vivo* by immunohistochemical staining (Fig. 7C) and Western blotting assay (Fig. 7D). Consistent with the *in vitro* studies, nanoparticle encapsulation enhanced the inhibitory effects of SP141 on MDM2 protein expression, whereas SP141FcNP showed the strongest inhibitory effects. Similar results were observed in TUNEL staining (Fig. 7C) and p21 protein expression level (Fig. 7D).

SP141FcNP was further examined for the effects on metastasis in mice bearing MDA-MB-231 orthotopic tumors (Fig. 7E). Necropsy showed that 9 out of 10 mice from control group developed metastatic lesions in the lungs. The incidence of lung metastasis in the SP141-treated and SP141NP-treated mice was 4/10 and 2/10, respectively. However, only 1 out of 10 mice treated with 80 mg/kg of SP141FcNP was found to have metastatic lesions and no lung metastasis was observed in all mice treated with 160 mg/kg of SP141FcNP. These results were confirmed by histopathological examinations (Fig. 7F). No significant abnormalities were found in any other major organs (brain, heart, liver, spleen, and kidney) from these mice, indicating the absence of host toxicity (Fig. 8). These findings indicated that SP141FcNP exerted enhanced inhibitory effects on both tumor growth and metastasis without host toxicity.

4. Discussion

In the present study, we developed, characterized, and assessed a biodegradable and biocompatible nanoformulation with surface functionalization with IgG Fc portion for oral delivery of the small molecule MDM2 inhibitor SP141. We have demonstrated several important findings. First, SP141FcNP is developed by employing biodegradable and biocompatible copolymers and shows a characteristic of biphasic release pattern. Second, this nanoformulation protects SP141 from premature degradation in the stomach and increases its transepithelial transport *in vitro* and *in vivo* with the involvement of FcRn-mediated transcytosis. Third, this nano-delivery system improves the cellular uptake of SP141 *in vitro* and *in vivo* via, at least in part, FcRn-mediated endocytosis. Fourth, the nanoformulation improves the oral bioavailability of SP141 with extended blood circulation time and increases its accumulation in tumors and other tissues *in vivo*. Fifth, SP141FcNP displays the enhanced inhibitory effects on tumor growth and metastasis and MDM2 expression *in vitro* and *in vivo*, independent of p53. Finally, SP141FcNP does not show significant host toxicity at the effective doses. These results demonstrate that Fc-conjugated nanoparticles are safe and effective for oral delivery of SP141, and may accelerate the clinical translation of SP141 for breast cancer treatment.

Oral administration of the anticancer therapeutic agents is always considered as the most convenient and preferred route for patient care [25, 42]. Administration of chemotherapy via i.v. injection could lead to high serum concentration above the maximum tolerable concentration as well as fast excretion from the systemic circulation, resulting in serious side effects and limited efficacy. Thereby, it is expected that oral chemotherapy can give a stable and sustained release of the drug and maintain a moderate concentration in the circulation. However, most anticancer drugs are not orally bioavailable because of their low absorption and interactive properties in the gastrointestinal tract, such as the newly discovered MDM2 inhibitor SP141 [12, 14]. Due to the low oral bioavailability and instability under harsh conditions, SP141 showed limited efficacy *in vivo* after oral administration. Therefore, new strategies are urgently needed for oral delivery of this anticancer compound.

Nanotechnology-based drug delivery has been applied to mitigate the difficulty associated with the administration of conventional anticancer drugs [20, 21, 42]. Several novel and effective anticancer nanomedicines have been successfully developed, leading to the optimization of the pharmaceutical action of drugs and the reduction of their adverse effects [20, 21]. Nevertheless, safe and effective oral anticancer nanomedicine is still lacking. IgG-based drugs have been considered as the most successful protein therapeutics due to FcRn, the central regulator of IgGmediated intestinal absorption and serum persistence [27, 28]. FcRn is involved in regulating autoimmune disease, mucosal immunity, and tumor immune surveillance, and it has been demonstrated as a molecular target for drug delivery and therapy [27, 28]. IgG Fc-fusion is one of the most clinically successful strategies for extending the protein half-life, and many Fc-fusion proteins in clinical use have a long half-life of up to 13 days in human bodies [43]. In addition, antibody engineering approaches, *e.g.* Abdegs, have been developed to prevent and disrupt the endogenous IgG-FcRn interaction, reducing the IgG level in serum for treating autoimmunity [44, 45]. More recently, IgG Fc fragment-conjugated nanoparticles have been prepared to increase the oral bioavailability of insulin as well as its tissue accumulation [33, 34]. However, the pharmacological properties and therapeutic efficacy of Fc-conjugated nanomedicine in human cancer models, especially, the tumor uptake and accumulation have not been determined yet.

Several *in vitro* and *in vivo* studies were employed to demonstrate the pivotal role of Fc-conjugation in the enhanced intestinal absorption and increased tumor uptake of SP141FcNP. First, the stability studies of SP141FcNP showed that Fc-conjugation did not affect the stability and release pattern of the nanoparticles. Second, the results from Caco2 cell monolayer permeability assay suggested that Fc-conjugation could improve the intestinal absorption of the intact SP141FcNP. The competition studies using free Fc fragments further illustrated the critical role of Fc-conjugation in the FcRn-mediated transcytosis of SP141FcNP. Third, the cellular uptake studies of SP141FcNP in both intestinal epithelial cells and breast cancer cells indicated that FcRn-mediated endocytosis contributed to the increased uptake of Fc-conjugated nanoparticles. Fourth, the intestinal uptake studies using both CD-1 mice and nude mice demonstrated the increased cellular uptake of FcNP *in vivo*, implying that there was no strain-related variation. As seen from the *in vitro* studies, the enhanced intestinal absorption was also observed in different *in vivo* models, confirming the importance of Fc-conjugation for this nanoformulation.

Furthermore, *in vitro* and *in vivo* preclinical models of human breast cancer have been utilized to evaluate the safety, bioavailability, and efficacy of SP141FcNP. To demonstrate the anticancer efficacy, MCF7 and MDA-MB-231 breast cancer cell lines with different genetic backgrounds (FcRn, MDM2, and p53) and MDA-MB-231 orthotopic model were utilized for the *in vitro* and *in vivo* evaluation, respectively. Importantly, SP141FcNP did not show significant adverse effects *in vivo*, as demonstrated in both short-term toxicity studies using CD-1 mice and efficacy studies in tumor-bearing nude mice. To evaluate the pharmacokinetics and tumor uptake of SP141FcNP, both CD-1 mice and nude mice bearing MDA-MB-231 orthotopic tumors were employed for determining the SP141 concentrations in plasma, tumor, and various tissues after oral administration. The real-time biodistribution of DiD-FcNP and its tumor and tissue accumulation were examined using *in vivo* and *ex vivo* imaging in both CD-1 mice and tumor-bearing nude mice. Our findings demonstrated that SP141 exerted improved pharmacokinetic and pharmacodynamic profiles in Fc-conjugated nanoformulation in the treatment of breast cancer, indicating that the nano-oral delivery system had the capability of overcoming the poor oral absorption of SP141.

Of note, due to the existence of inter-species human IgG-mouse FcRn interaction, our results obtained from both CD1 and nude mice may not exactly reflect the pharmacokinetics. Recent studies have enhanced our understanding of the inter-species IgG Fc-FcRn interactions and the underlying mechanisms of action. IgG from various species, including human has significant cross-species differences in its interaction with FcRn from other species [46]. Human FcRn is rigorous in its binding to human IgG, and it does not interact well with mouse IgG [47]. In contrast to human FcRn, mouse FcRn is promiscuous in its binding specificity and interacts with IgG from various species, including human IgG [47]. Although these findings explain the improved oral bioavailability and pharmacokinetics of human IgG-based drugs in mice, they also raise questions concerning the validity of using mouse models to predict the safety, pharmacokinetic, and efficacy of these human IgG-based drugs, such as SP141FcNPs. It has been reported that the distinct cross-species behavior of FcRn (human or mouse) could be attributed to the less exposed position of Trp133 and/or deletion of residues 85 and 86 (located in the α1 domain) in human FcRn [48–49]. Although the underlying mechanism is not completely investigated yet, these findings suggest that the circulating mouse IgG may not competitively impede the targeting of human IgG-based drugs in mouse models *in vivo* and these human IgG-based drugs may not be rapidly cleared from mouse circulation, leading to a longer half-life and better efficacy than that in human body. Therefore, the mouse models may not be reliably used to extrapolate the half-life and efficacy of human IgG-based drugs. Nevertheless, we have carefully considered these caveats in our studies. The present study was designed to provide proof-of-principle for developing Fc-conjugated nanoparticle platform for oral delivery of SP141, and these data at least provided the evidence on the safety and effectiveness of SP141FcNP in preclinical settings. In addition, in the present study, our *in vivo* animal studies have also been complemented by using human Caco2 and breast cancer MCF7 and MDA-MB-231 cell lines, which demonstrate the specific interaction between human FcNP and human FcRn as well as improved cell and tumor uptake and enhanced activity.

Moreover, IgG Fc fusion proteins have high therapeutic potency, long serum half-life and lack of off-target toxicity [43]. However, considering that FcRn is commonly expressed in

various normal organs and tissues, the specific Fc-FcRn binding may result in the exaggerated accumulation and amplified pharmacology of the Fc fusion proteins at these non-therapeutic sites. The likelihood of adverse effects occurring in these normal organs and tissues still remains and a thorough understanding of their pharmacological effects and mechanism(s) of action is certainly required. Therefore, further investigations are needed to determine the efficacy, safety, and molecular mechanisms of SP141FcNP using more clinically relevant models of human breast cancer, including FcRn knockout model.

5. Conclusion

Our newly developed SP141FcNP displays controllable nanoformulation properties, improved oral bioavailability, increased tumor uptake and enhanced efficacy *in vitro* and *in vivo* in comparison to free SP141 and non-targeted SP141NP, with no apparent host toxicity. While further investigation is needed, these data demonstrate the strong potential of SP141FcNP as a safe and efficient oral delivery system for SP141, providing critical information for future clinical translation of this nanomedicine for breast cancer therapy.

Supplementary Material

Refer to Web version on PubMed Central for supplementary material.

Acknowledgments

References

1. Ojesina AI, Lichtenstein L, Freeman SS, Pedamallu CS, Imaz-Rosshandler I, Pugh TJ, et al. Landscape of genomic alterations in cervical carcinomas. Nature. 2014; 506:371–375. [PubMed: 24390348]

2. Alexandrov LB, Nik-Zainal S, Wedge DC, Aparicio SA, Behjati S, Biankin AV, et al. Signatures of mutational processes in human cancer. Nature. 2013; 500:415–421. [PubMed: 23945592]

3. Vinagre J, Almeida A, Populo H, Batista R, Lyra J, Pinto V, et al. Frequency of TERT promoter mutations in human cancers. Nat Commun. 2013; 4:2185. [PubMed: 23887589]

4. Santarius T, Shipley J, Brewer D, Stratton MR, Cooper CS. A census of amplified and overexpressed human cancer genes. Nat Rev Cancer. 2010; 10:59–64. [PubMed: 20029424]

5. Muller PA, Vousden KH. p53 mutations in cancer. Nat Cell Biol. 2013; 15:2–8. [PubMed: 23263379]

6. Wade M, Li YC, Wahl GM. MDM2, MDMX and p53 in oncogenesis and cancer therapy. Nat Rev Cancer. 2013; 13:83–96. [PubMed: 23303139]

7. Nag S, Zhang X, Srivenugopal KS, Wang MH, Wang W, Zhang R. Targeting MDM2-p53 interaction for cancer therapy: are we there yet? Curr Med Chem. 2014; 21:553–574. [PubMed: 24180275]

8. Li Q, Lozano G. Molecular pathways: targeting Mdm2 and Mdm4 in cancer therapy. Clin Cancer Res. 2013; 19:34–41. [PubMed: 23262034]

9. Vassilev LT, Vu BT, Graves B, Carvajal D, Podlaski F, Filipovic Z, et al. In vivo activation of the p53 pathway by small-molecule antagonists of MDM2. Science. 2004; 303:844–848. [PubMed: 14704432]

10. Issaeva N, Bozko P, Enge M, Protopopova M, Verhoef LG, Masucci M, et al. Small molecule RITA binds to p53, blocks p53-HDM-2 interaction and activates p53 function in tumors. Nat Med. 2004; 10:1321–1328. [PubMed: 15558054]

11. Shangary S, Qin D, McEachern D, Liu M, Miller RS, Qiu S, et al. Temporal activation of p53 by a specific MDM2 inhibitor is selectively toxic to tumors and leads to complete tumor growth inhibition. Proc Natl Acad Sci U S A. 2008; 105:3933–3938. [PubMed: 18316739]

12. Wang W, Qin JJ, Voruganti S, Srivenugopal KS, Nag S, Patil S, et al. The pyrido[b]indole MDM2 inhibitor SP-141 exerts potent therapeutic effects in breast cancer models. Nat Commun. 2014; 5:5086. [PubMed: 25271708]

13. Qin JJ, Wang W, Voruganti S, Wang H, Zhang WD, Zhang R. Identification of a new class of natural product MDM2 inhibitor: In vitro and in vivo anti-breast cancer activities and target validation. Oncotarget. 2015; 6:2623–2640. [PubMed: 25739118]

14. Wang W, Qin JJ, Voruganti S, Wang MH, Sharma H, Patil S, et al. Identification of a new class of MDM2 inhibitor that inhibits growth of orthotopic pancreatic tumors in mice. Gastroenterology. 2014; 147:893–902. e892. [PubMed: 25016295]

15. Gamboa JM, Leong KW. In vitro and in vivo models for the study of oral delivery of nanoparticles. Adv Drug Deliv Rev. 2013; 65:800–810. [PubMed: 23415952]

16. Wicki A, Witzigmann D, Balasubramanian V, Huwyler J. Nanomedicine in cancer therapy: challenges, opportunities, and clinical applications. J Control Release. 2015; 200:138–157. [PubMed: 25545217]

17. Mei L, Zhang Z, Zhao L, Huang L, Yang XL, Tang J, et al. Pharmaceutical nanotechnology for oral delivery of anticancer drugs. Adv Drug Deliv Rev. 2013; 65:880–890. [PubMed: 23220325]

18. Juliano R. Nanomedicine: is the wave cresting? Nat Rev Drug Discov. 2013; 12:171–172. [PubMed: 23449291]

19. Cortes JE, Goldberg SL, Feldman EJ, Rizzeri DA, Hogge DE, Larson M, et al. Phase II, multicenter, randomized trial of CPX-351 (cytarabine:daunorubicin) liposome injection versus intensive salvage therapy in adults with first relapse AML. Cancer. 2015; 121:234–242. [PubMed: 25223583]

20. Xu X, Ho W, Zhang X, Bertrand N, Farokhzad O. Cancer nanomedicine: from targeted delivery to combination therapy. Trends Mol Med. 2015; 21:223–232. [PubMed: 25656384]

21. Lytton-Jean AK, Kauffman KJ, Kaczmarek JC, Langer R. Cancer nanotherapeutics in clinical trials. Cancer Treat Res. 2015; 166:293–322. [PubMed: 25895874]

22. Shan W, Zhu X, Liu M, Li L, Zhong J, Sun W, et al. Overcoming the diffusion barrier of mucus and absorption barrier of epithelium by self-assembled nanoparticles for oral delivery of insulin. ACS Nano. 2015; 9:2345–2356. [PubMed: 25658958]

23. Varamini P, Toth I. Recent advances in oral delivery of peptide hormones. Expert Opin Drug Deliv. 2016:1–16.

24. Voruganti S, Qin JJ, Sarkar S, Nag S, Walbi IA, Wang S, et al. Oral nano-delivery of anticancer ginsenoside 25-OCH3-PPD, a natural inhibitor of the MDM2 oncogene: Nanoparticle preparation, characterization, in vitro and in vivo anti-prostate cancer activity, and mechanisms of action. Oncotarget. 2015; 6:21379–21394. [PubMed: 26041888]

25. Pridgen EM, Alexis F, Farokhzad OC. Polymeric nanoparticle drug delivery technologies for oral delivery applications. Expert Opin Drug Deliv. 2015; 12:1459–1473. [PubMed: 25813361]

26. Ensign LM, Cone R, Hanes J. Oral drug delivery with polymeric nanoparticles: the gastrointestinal mucus barriers. Adv Drug Deliv Rev. 2012; 64:557–570. [PubMed: 22212900]

27. Sockolosky JT, Szoka FC. The neonatal Fc receptor, FcRn, as a target for drug delivery and therapy. Adv Drug Deliv Rev. 2015; 91:109–124. [PubMed: 25703189]

28. Rath T, Baker K, Dumont JA, Peters RT, Jiang H, Qiao SW, et al. Fc-fusion proteins and FcRn: structural insights for longer-lasting and more effective therapeutics. Crit Rev Biotechnol. 2015; 35:235–254. [PubMed: 24156398]

29. Akilesh S, Christianson GJ, Roopenian DC, Shaw AS. Neonatal FcR expression in bone marrow-derived cells functions to protect serum IgG from catabolism. J Immunol. 2007; 179:4580–4588. 179/7/4580 [pii]. [PubMed: 17878355]

30. Montoyo HP, Vaccaro C, Hafner M, Ober RJ, Mueller W, Ward ES. Conditional deletion of the MHC class I-related receptor FcRn reveals the sites of IgG homeostasis in mice. Proc Natl Acad Sci U S A. 2009; 106:2788–2793. [PubMed: 19188594]

31. Baker K, Qiao SW, Kuo TT, Aveson VG, Platzer B, Andersen JT, et al. Neonatal Fc receptor for IgG (FcRn) regulates cross-presentation of IgG immune complexes by CD8-CD11b+ dendritic cells. Proc Natl Acad Sci U S A. 2011; 108:9927–9932. [PubMed: 21628593]

32. Andersen JT, Pehrson R, Tolmachev V, Daba MB, Abrahmsen L, Ekblad C. Extending half-life by indirect targeting of the neonatal Fc receptor (FcRn) using a minimal albumin binding domain. J Biol Chem. 2011; 286:5234–5241. [PubMed: 21138843]

33. Vllasaliu D, Alexander C, Garnett M, Eaton M, Stolnik S. Fc-mediated transport of nanoparticles across airway epithelial cell layers. J Control Release. 2012; 158:479–486. [PubMed: 22200577]

34. Pridgen EM, Alexis F, Kuo TT, Levy-Nissenbaum E, Karnik R, Blumberg RS, et al. Transepithelial transport of Fc-targeted nanoparticles by the neonatal fc receptor for oral delivery. Sci Transl Med. 2013; 5:213ra167.

35. Xin H, Sha X, Jiang X, Chen L, Law K, Gu J, et al. The brain targeting mechanism of Angiopep-conjugated poly(ethylene glycol)-co-poly(epsilon-caprolactone) nanoparticles. Biomaterials. 2012; 33:1673–1681. [PubMed: 22133551]

36. Nag S, Qin JJ, Voruganti S, Wang MH, Sharma H, Patil S, et al. Development and validation of a rapid HPLC method for quantitation of SP-141, a novel pyrido[b]indole anticancer agent, and an initial pharmacokinetic study in mice. Biomed Chromatogr. 2015; 29:654–663. [PubMed: 25294254]

37. Qin JJ, Jin HZ, Huang Y, Zhang SD, Shan L, Voruganti S, et al. Selective cytotoxicity, inhibition of cell cycle progression, and induction of apoptosis in human breast cancer cells by sesquiterpenoids from Inula lineariifolia Turcz. Eur J Med Chem. 2013; 68:473–481. [PubMed: 24044895]

38. Qin JJ, Wang W, Voruganti S, Wang H, Zhang WD, Zhang R. Inhibiting NFAT1 for breast cancer therapy: New insights into the mechanism of action of MDM2 inhibitor JapA. Oncotarget. 2015; 6:33106–33119. [PubMed: 26461225]

39. Wang W, Cheng J, Qin JJ, Voruganti S, Nag S, Fan J, et al. RYBP expression is associated with better survival of patients with hepatocellular carcinoma (HCC) and responsiveness to chemotherapy of HCC cells in vitro and in vivo. Oncotarget. 2014; 5:11604–11619. [PubMed: 25344099]

40. Voruganti S, Xu F, Qin JJ, Guo Y, Sarkar S, Gao M, et al. RYBP predicts survival of patients with non-small cell lung cancer and regulates tumor cell growth and the response to chemotherapy. Cancer Lett. 2015; 369:386–395. [PubMed: 26404750]

41. Nag S, Qin JJ, Patil S, Deokar H, Buolamwini JK, Wang W, et al. A quantitative LC-MS/MS method for determination of SP-141, a novel pyrido[b]indole anticancer agent, and its application to a mouse PK study. J Chromatogr B Analyt Technol Biomed Life Sci. 2014; 969:235–240.

42. Thanki K, Gangwal RP, Sangamwar AT, Jain S. Oral delivery of anticancer drugs: challenges and opportunities. J Control Release. 2013; 170:15–40. [PubMed: 23648832]

43. Suzuki T, Ishii-Watabe A, Tada M, Kobayashi T, Kanayasu-Toyoda T, Kawanishi T, et al. Importance of neonatal FcR in regulating the serum half-life of therapeutic proteins containing the Fc domain of human IgG1: a comparative study of the affinity of monoclonal antibodies and Fc-fusion proteins to human neonatal FcR. J Immunol. 2010; 184:1968–1976. [PubMed: 20083659]

44. Vaccaro C, Zhou J, Ober RJ, Ward ES. Engineering the Fc region of immunoglobulin G to modulate in vivo antibody levels. Nat Biotechnol. 2005; 23:1283–1288. [PubMed: 16186811]

45. Patel DA, Puig-Canto A, Challa DK, Perez Montoyo H, Ober RJ, Ward ES. Neonatal Fc receptor blockade by Fc engineering ameliorates arthritis in a murine model. J Immunol. 2011; 187:1015–1022. [PubMed: 21690327]

46. Andersen JT, Daba MB, Berntzen G, Michaelsen TE, Sandlie I. Cross-species binding analyses of mouse and human neonatal Fc receptor show dramatic differences in immunoglobulin G and albumin binding. J Biol Chem. 2010; 285:4826–4836. [PubMed: 20018855]

47. Ober RJ, Radu CG, Ghetie V, Ward ES. Differences in promiscuity for antibody-FcRn interactions across species: implications for therapeutic antibodies. Int Immunol. 2001; 13:1551–1559. [PubMed: 11717196]

48. Martin WL, West AP Jr, Gan L, Bjorkman PJ. Crystal structure at 2.8 A of an FcRn/heterodimeric Fc complex: mechanism of pH-dependent binding. Mol Cell. 2001; 7:867–877. [PubMed: 11336709]

49. West AP Jr, Bjorkman PJ. Crystal structure and immunoglobulin G binding properties of the human major histocompatibility complex-related Fc receptor. Biochemistry. 2000; 39:9698–9708. [PubMed: 10933786]
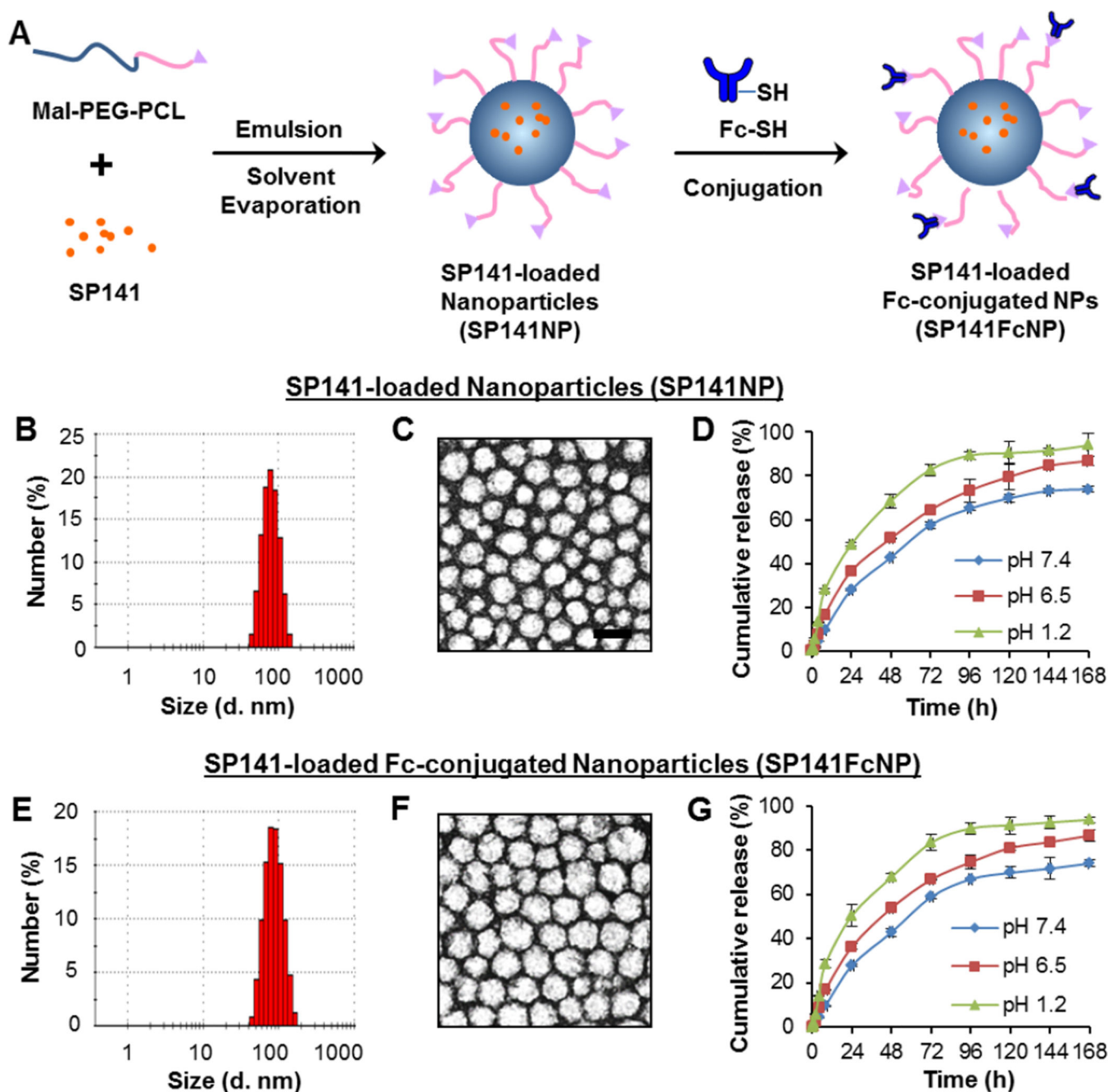
Fig. 1. Design, preparation, and characterization of SP141FcNP

(**A**) The strategy of constructing SP141-loaded Fc-conjugated nanoparticles (SP141FcNP). (**B**) Particle size and size distribution and (**C**) morphology of non-targeted SP141NP determined by dynamic light scattering (DLS) and transmission electron microscopy (TEM) (scale bar, 100 nm), respectively. (**D**) The cumulative release kinetics of SP141 from SP141NP in simulated gastric fluid (pH 1.2), simulated intestinal fluid (pH 6.5) without enzymes and PBS (pH 7.4) (Mean ± SEM; n = 9 for each data point). (**E**) Particle size and size distribution and (**F**) morphology of SP141FcNP determined by DLS and TEM, respectively. (**G**) The cumulative release kinetics of SP141 from SP141FcNP in simulated

gastric fluid (pH 1.2), simulated intestinal fluid (pH 6.5) without enzymes and PBS (pH 7.4) (Mean ± SEM; n = 9 for each data point). The concentration unit for SP141NP and SP141FcNP is SP141 equivalent in all experiments. All experiments were repeated at least three times.
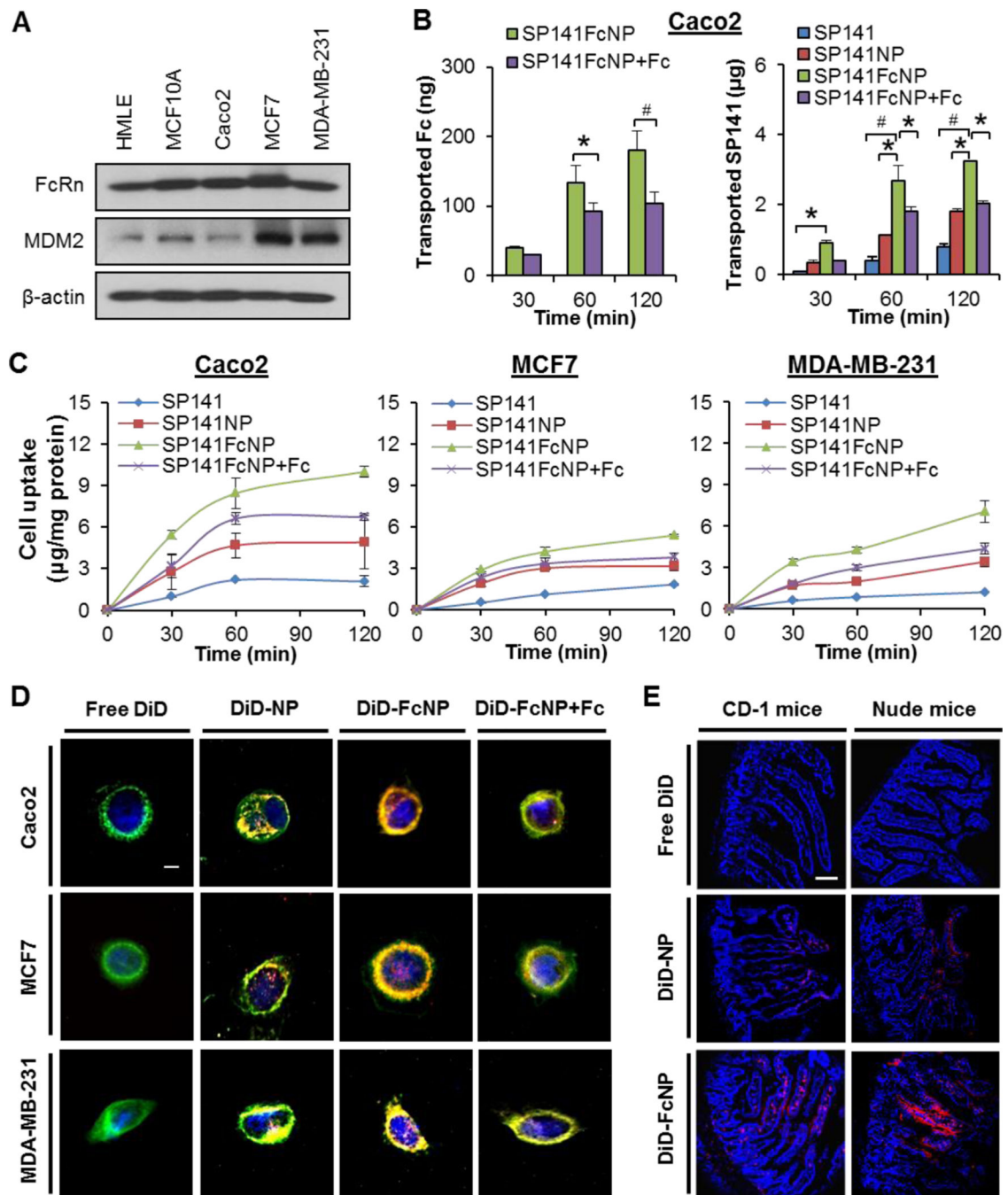
Fig. 2. Permeability and cellular uptake of SP141FcNP

(**A**) Western blotting analyses of FcRn and MDM2 in normal human breast (HMLE and MCF-10A) cell lines, human intestinal epithelial (Caco2) cells and breast cancer (MCF7 and MDA-MB-231) cell lines. (**B**) The permeation of free SP141, nontargeted SP141NP, and SP141FcNP in the absence and presence of free Fc fragments from apical to basolateral across Caco2 cell monolayers at 37°C, presented as the amount of Fc (left panel) and SP141 (right panel) transported. (**C**) Cells were treated with free SP141, SP141NP, and SP141FcNP in the absence and presence of free Fc fragments for 2 h. SP141 was extracted and quantified

by an HPLC analysis and normalized to the protein content. The concentration unit for SP141NP and SP141FcNP is SP141 equivalent in all experiments. (**D**) Cells were incubated with free DiD, non-targeted DiD-NP, and DiD-FcNP in the absence and presence of free Fc fragments for 2 h, then the cellular uptake was monitored by a fluorescence microscope (scale bar, 5 μm). Cell membrane was stained with CellVue® dye and cell nuclei were stained with DAPI (blue). All assays described above were performed in triplicate and all the experiments were repeated at least three times (Mean ± SEM, n = 9 for each data point, two-sided Student's t-test, $*P < 0.05$, $\#P < 0.01$). (**E**) Free DiD, DiD-NP, and DiD-FcNP were administered to fasted CD-1 and nude mice by oral gavage and the intestines were collected for sectioning and imaging 2 h after administration. The panels are confocal fluorescence images of 20 μm sections of mouse duodenum. Cell nuclei were stained with DAPI (blue). All images represented the series of sections (scale bar, 50 μm; n = 3 animals per group).
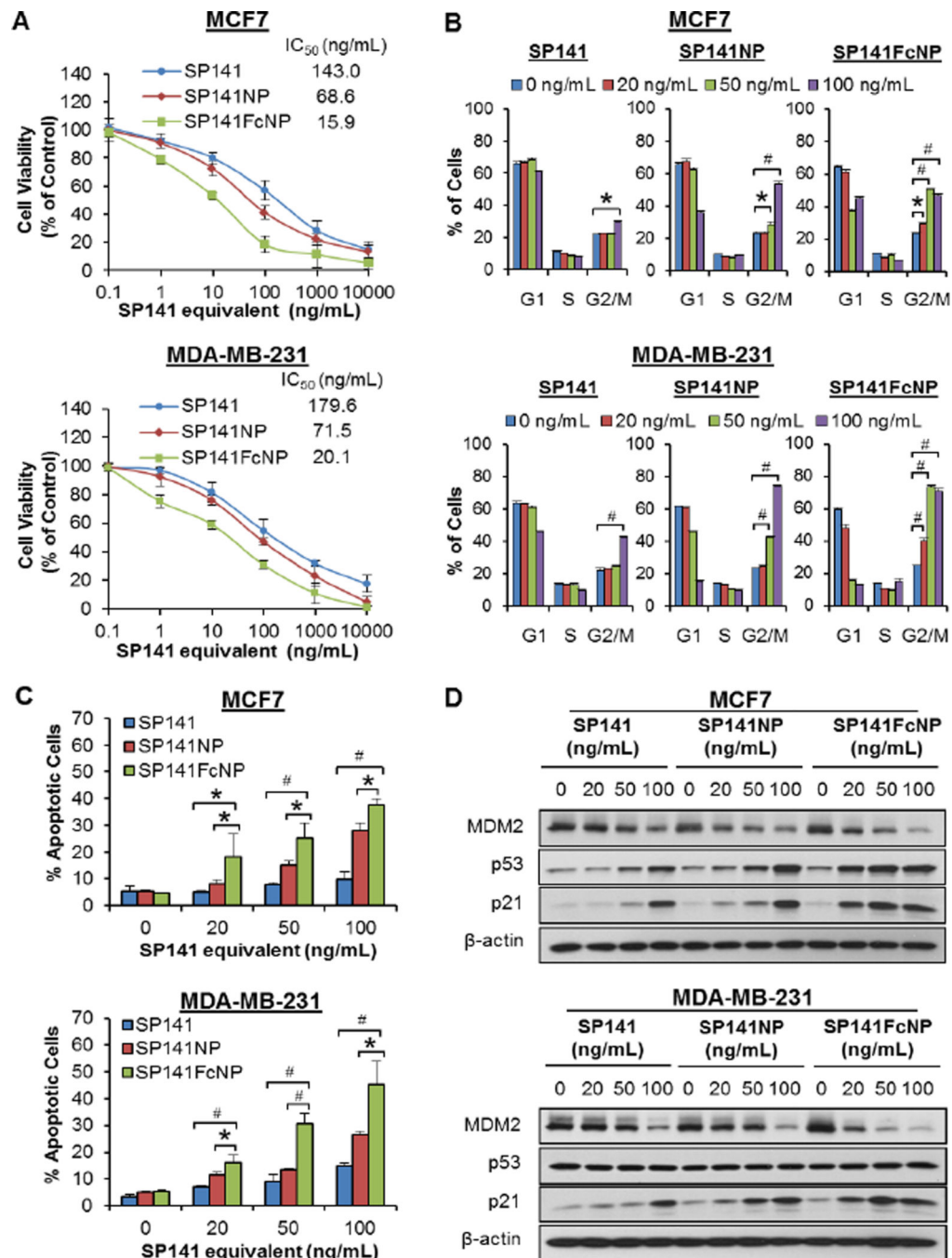
Fig. 3. *In vitro* anti-breast cancer activity of SP141FcNP

MCF7 and MDA-MB-231 cells were exposed to various concentrations of SP141, SP141NP, and SP141FcNP for (**A**) 72 h for determination of the cell viability; (**B**) 24 h for cell cycle distribution assay; (**C**) 48 h for the cell apoptosis assay; and (**D**) 24 h to determine the expression levels of various proteins by Western blotting analyses. The concentration unit for SP141NP and SP141FcNP is SP141 equivalent in all experiments. All assays were performed in triplicate, and all the experiments were repeated at least three times (Mean ± SEM, n = 9 for each data point, two-sided Student's t-test, *$P < 0.05$, #$P < 0.01$).
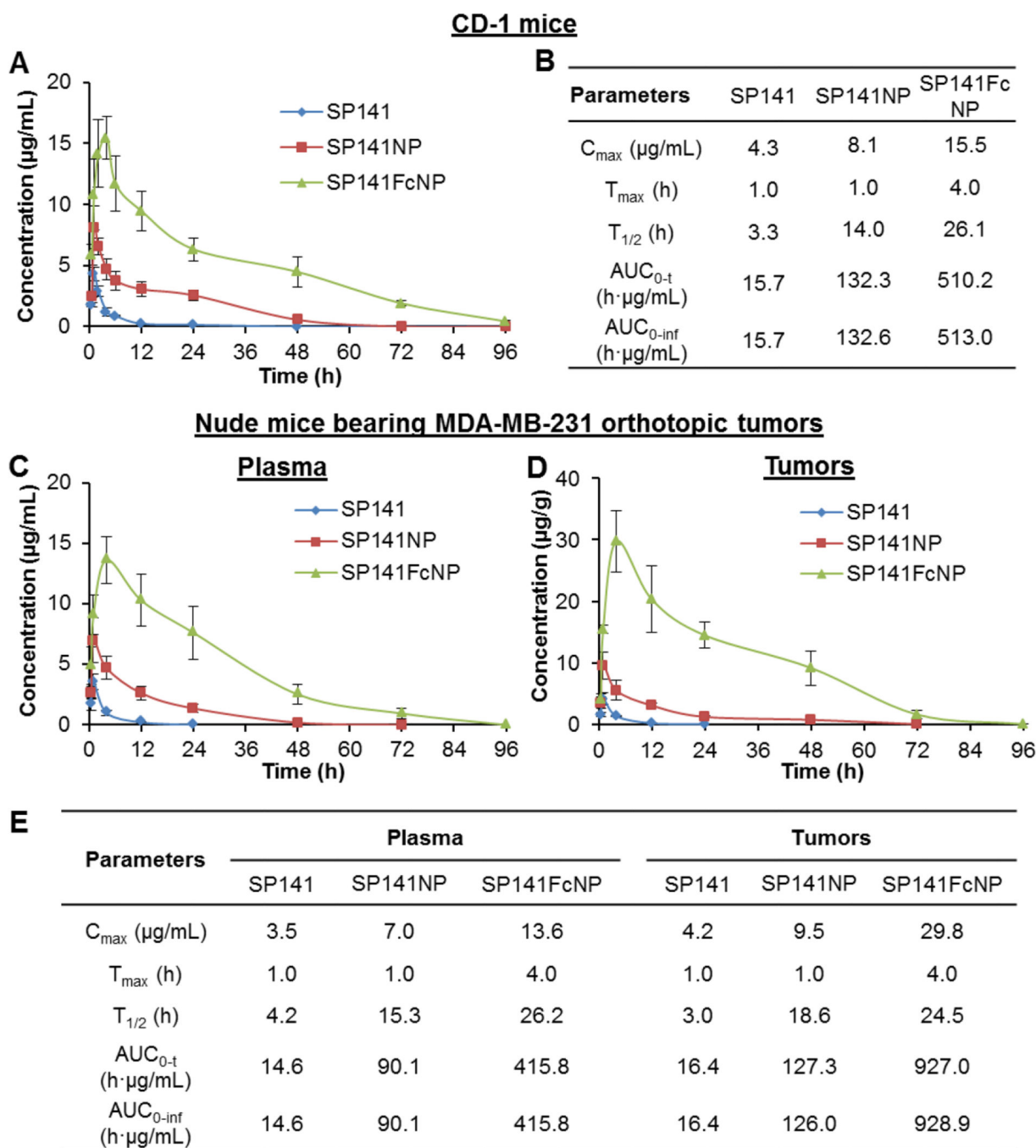
CD-1 mice

B

Parameters	SP141	SP141NP	SP141Fc NP
C_{max} (µg/mL)	4.3	8.1	15.5
T_{max} (h)	1.0	1.0	4.0
$T_{1/2}$ (h)	3.3	14.0	26.1
AUC_{0-t} (h·µg/mL)	15.7	132.3	510.2
AUC_{0-inf} (h·µg/mL)	15.7	132.6	513.0

Nude mice bearing MDA-MB-231 orthotopic tumors

E

Parameters	Plasma			Tumors		
	SP141	SP141NP	SP141FcNP	SP141	SP141NP	SP141FcNP
C_{max} (µg/mL)	3.5	7.0	13.6	4.2	9.5	29.8
T_{max} (h)	1.0	1.0	4.0	1.0	1.0	4.0
$T_{1/2}$ (h)	4.2	15.3	26.2	3.0	18.6	24.5
AUC_{0-t} (h·µg/mL)	14.6	90.1	415.8	16.4	127.3	927.0
AUC_{0-inf} (h·µg/mL)	14.6	90.1	415.8	16.4	126.0	928.9

Fig. 4. *In vivo* **pharmacokinetics and tumor uptake of SP141FcNP**
(**A**) The plasma concentrationtime curves following oral administration of free SP141 (160 mg/kg), non-targeted SP141NP (160 mg/kg), or SP141FcNP (160 mg/kg) to CD-1 mice. (**B**) The pharmacokinetic parameters of SP141, SP141NP, and SP141FcNP in CD-1 mice. (**C**) The plasma concentration-time curves following oral administration of SP141 (160 mg/kg), SP141NP (160 mg/kg), or SP141FcNP (160 mg/kg) to nude mice bearing MDA-MB-231 orthotopic tumors. (**D**) The time-dependent accumulation of SP141, SP141NP, and SP141FcNP in MDA-MB-231 orthotopic tumors. (**E**) The pharmacokinetic parameters of

SP141, SP141NP, and SP141FcNP in nude mice bearing MDA-MB-231 orthotopic tumors. The concentration unit for SP141NP and SP141FcNP is SP141 equivalent in all experiments (Mean ± SEM, n = 3 animals per group). C_{max}, the peak plasma or tumor concentration of SP141 after administration; T_{max}, time to reach C_{max}; $T_{1/2}$, the plasma or tumor half-life of SP141; AUC_{0-t}, the area under the concentration-time curve from the time zero to last measurable concentration; AUC_{0-inf}, the area under the concentration-time curve from the time zero to infinite time.

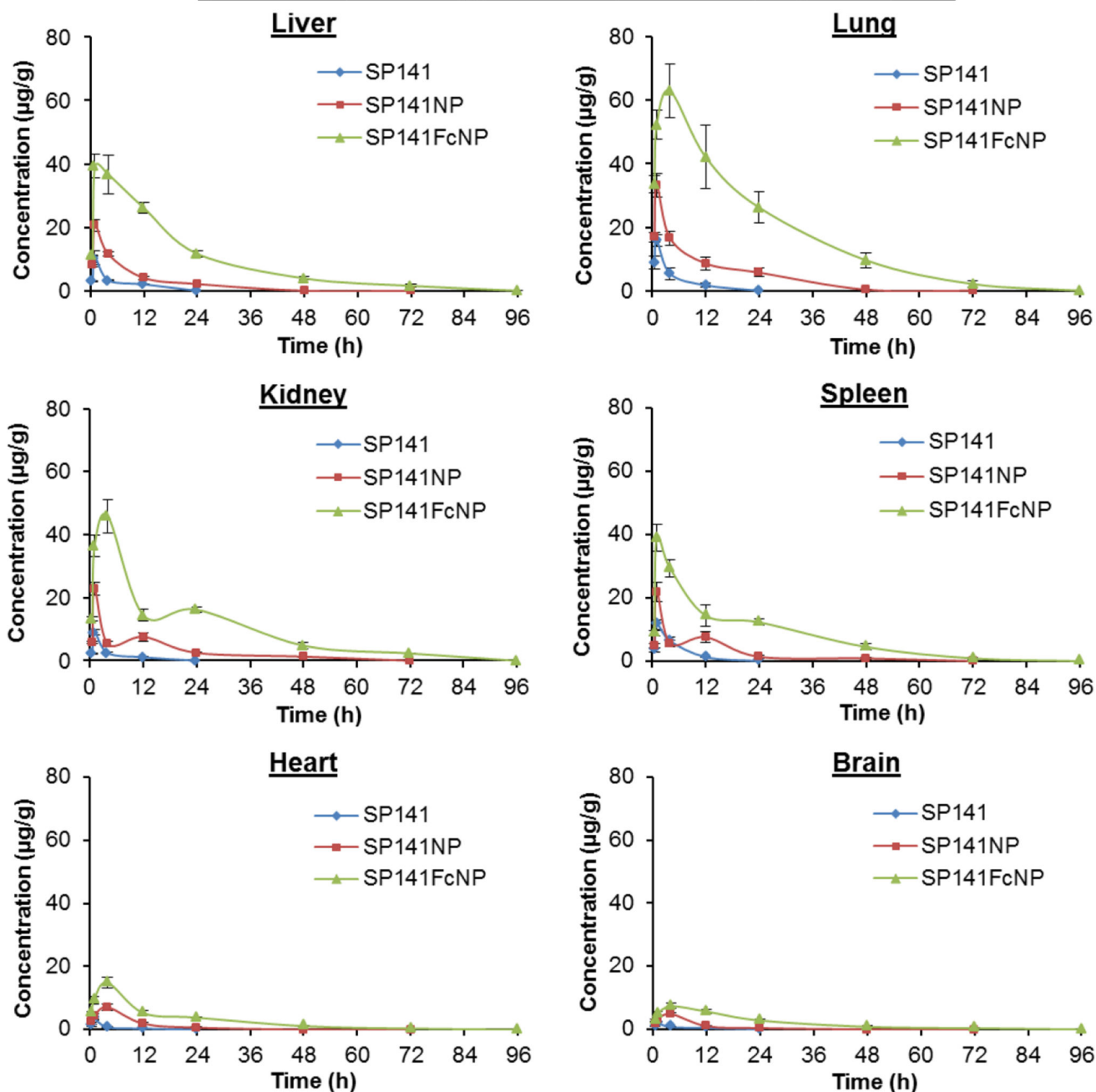# Nude mice bearing MDA-MB-231 orthotopic tumors

Fig. 5. Tissue biodistribution of SP141FcNP

The time-dependent distribution of SP141, SP141NP, and SP141FcNP in various tissues (liver, lung, kidney, spleen, heart, and brain) of nude mice bearing MDA-MB-231 orthotopic tumors after oral administration of free SP141 (160 mg/kg), non-targeted SP141NP (160 mg/kg), or SP141FcNP (160 mg/kg). The concentration unit for SP141NP and SP141FcNP is SP141 equivalent in all experiments (Mean ± SEM, n = 3 animals per group).
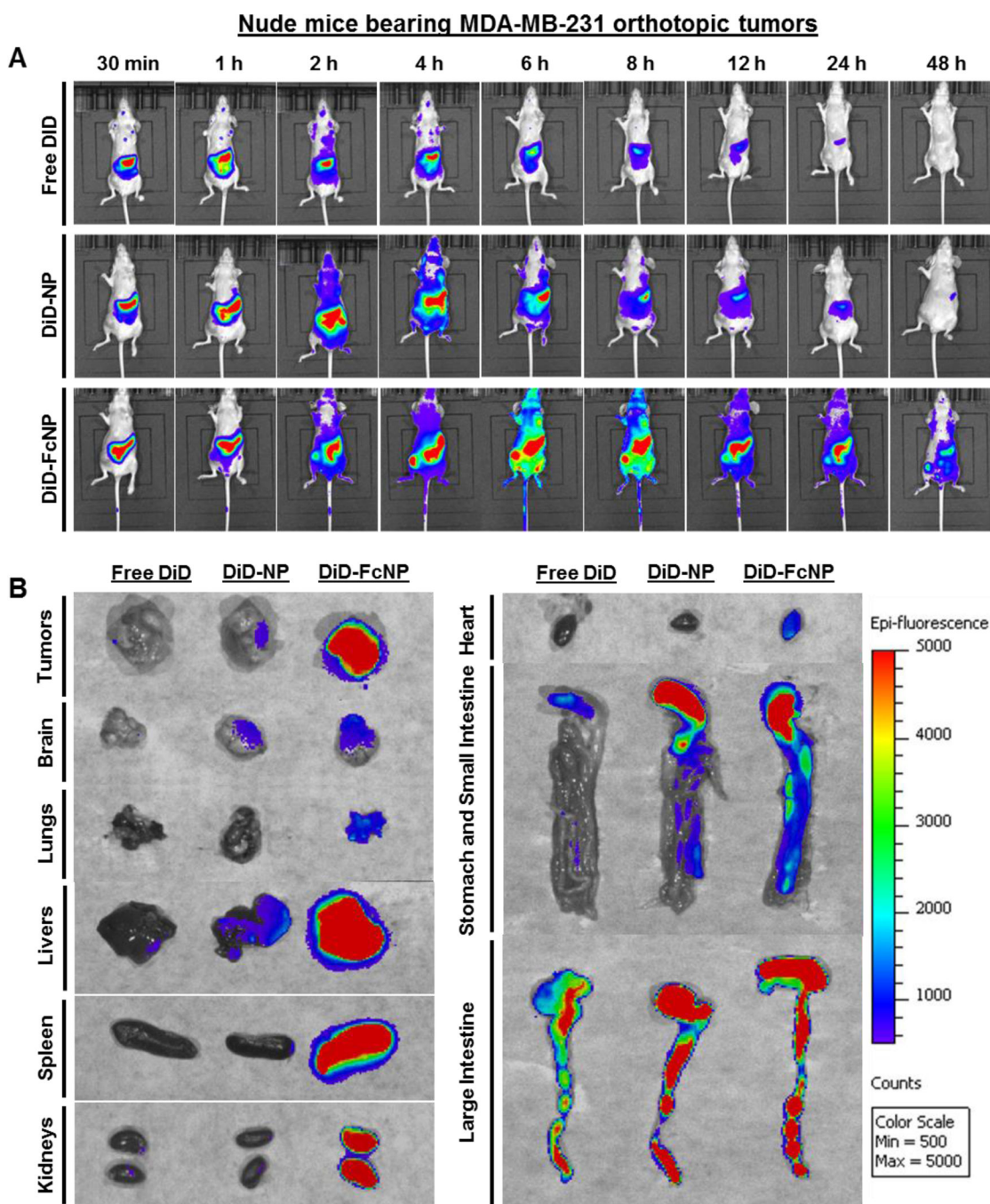
Fig. 6. Real-time tumor uptake and tissue biodistribution of FcNP
(**A**) *In vivo* images of time-dependent whole body imaging of nude mice bearing MDA-MB-231 orthotopic tumors after oral administration of free DiD (0.5 mg/kg), non-targeted DiD-NP (0.5 mg/kg), and DiD-FcNP (0.5 mg/kg) (n = 6 animals per group). (**B**) The *ex vivo* images of tumors and various tissues from tumor-bearing nude mice that were sacrificed at 6 h after oral administration. The concentration unit for DiD-NP and DiDFcNP is DiD equivalent in all experiments (n = 3 animals per group).
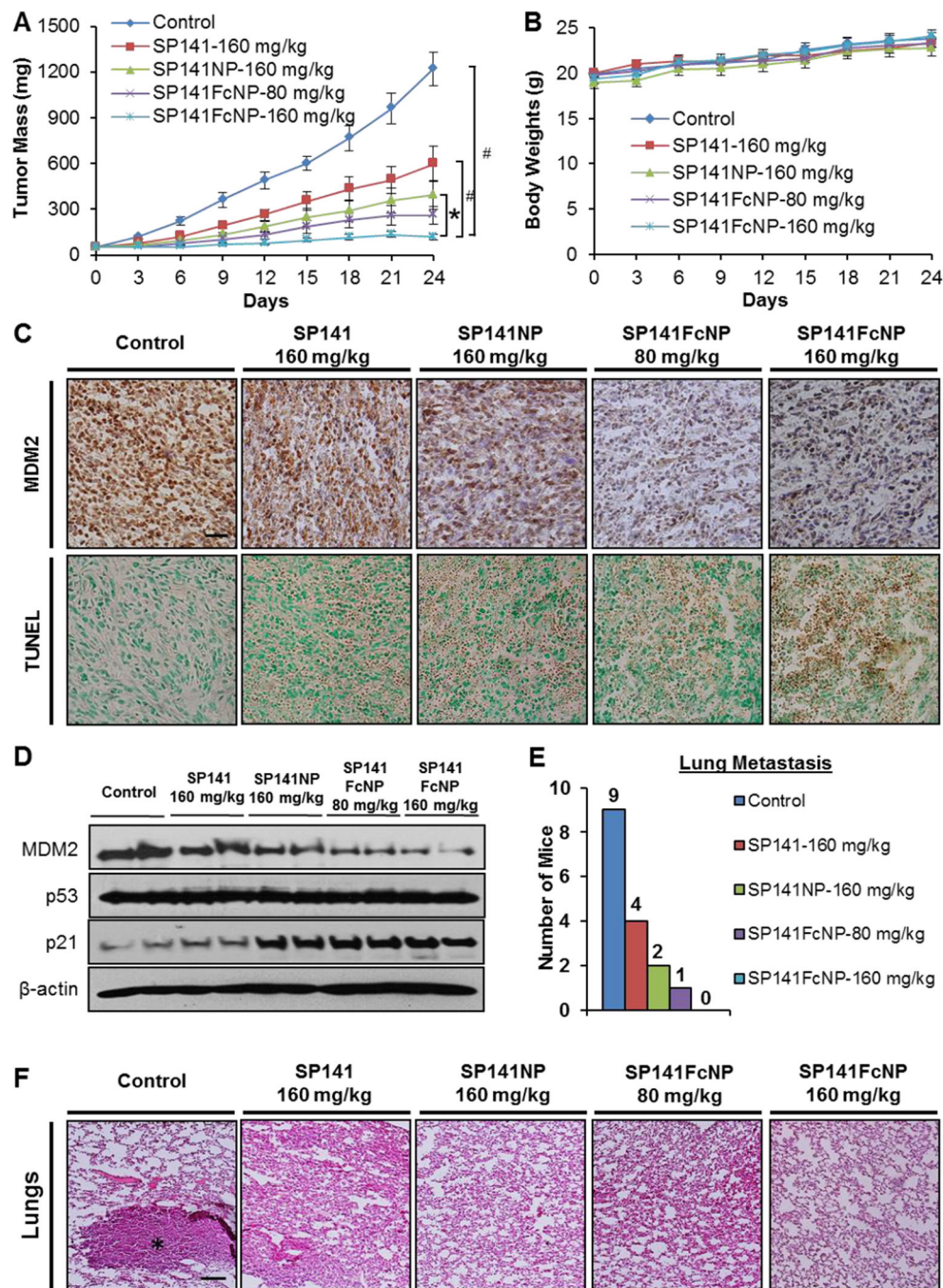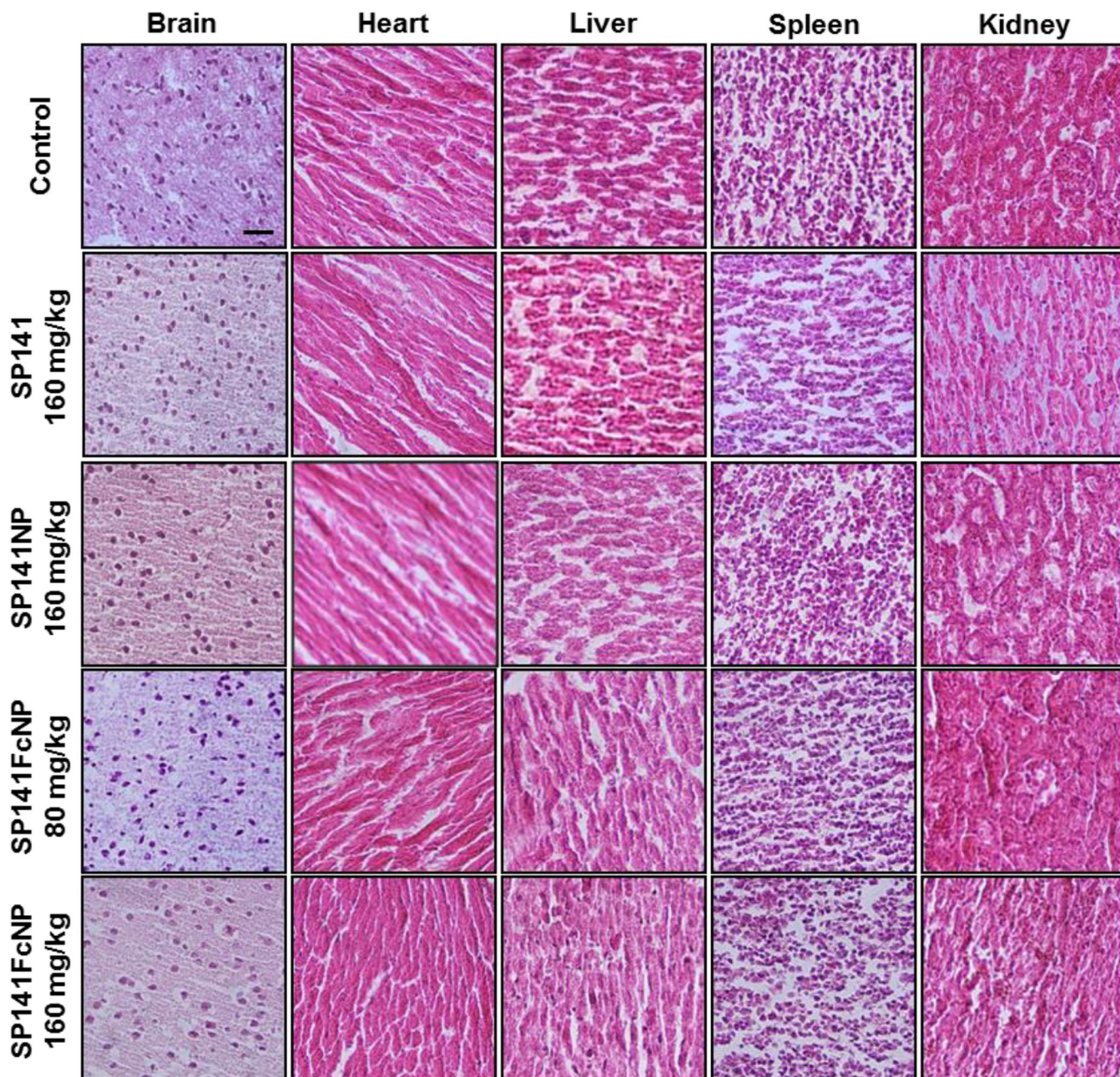
Fig. 7. *In vivo* efficacy of SP141FcNP

(**A**) Nude mice bearing MDA-MB-231 orthotopic tumors were treated with free SP141 (160 mg/kg), non-targeted SP141NP (160 mg/kg), or SP141FcNP (80 and 160 mg/kg) by oral administration 5 days/week for 24 days. The control mice received vehicle only. (**B**) All mice were monitored for changes in body weight as a surrogate marker of toxicity. At the termination of the experiments, tumors were excised and cut into multiple sections for (**C**) MDM2 immunohistochemical staining and TUNEL staining and (**D**) Western blotting analysis for the protein expression of MDM2, p53, and p21. All images represented the

series of sections (scale bar, 20 μm). (**E**) At the termination of the experiments, the mice were examined for tumor metastasis to various organs. The numbers of mice with metastasis to lungs were counted. (**F**) Lung tissues were carefully removed, and H&E staining of the paraffin sections of these tissues was performed. Black asterisk indicates the metastatic lesions (scale bar, 500 μm). The concentration unit for SP141NP and SP141FcNP is SP141 equivalent in all experiments (Mean ± SEM, n = 10 for each data point, two-sided Student's t-test, $*P < 0.05$, $\#P < 0.01$).

Nude mice bearing MDA-MB-231 orthotopic tumors

Fig. 8. SP141FcNP does not cause any significant host toxicity
Nude mice bearing MDA-MB-231 orthotopic tumors were treated with free SP141 (160 mg/
kg), non-targeted SP141NP (160 mg/kg), or SP141FcNP (80 and 160 mg/kg) by oral
administration 5 days/week for 24 days. The control mice received vehicle only. At the end
of experiments, H&E staining of the paraffin sections of various tissues (liver, kidneys,
spleen, heart, and brain) from mice was performed. All images represented the series of

sections (scale bar, 50 μm; n = 10 animals per group). The concentration unit for SP141NP and SP141FcNP is SP141 equivalent in all experiments.

Table 1

Physicochemical characterization of SP141NP and SP141FcNP

Formulation	Particle size (nm)	PDI	Zeta potential (mV)	DL%	EE%	CE%	SD
SP141NP	79.9±1.0	0.280±0.012	−7.2±0.2	16.5±1.4%	98.9±1.3%	N/A	N/A
SP141FcNP	85.5±2.8	0.291±0.013	−7.0±0.3	16.4±1.2%	98.6±1.1%	57.9%±1.8%	52±2

Abbreviations: SP141NP, SP141-loaded PEG-PCL nanoparticles; SP141FcNP, SP141-loaded Fc-conjugated PEG-PCL nanoparticles; PDI, Polydispersity; DL%, Drug Loading (%); EE%, Encapsulation Efficiency (% W/W); CE%, Fc Conjugation Efficiency (%); SD, Fc Surface Density